

Trajectories of a low Reynolds number treadmilling organism near a half-infinite no-slip wall

Kiori Obuse, Supervised by Jean-Luc Thiffeault

June-August 2010

Abstract

This project investigates the behaviour of a treadmilling microorganism in a two-dimensional unbounded domain with a half-infinite non-slip wall. The governing evolution equations for such a treadmilling organism are derived in an analytical form and trajectories of a microorganism for several different initial positions and heading directions are numerically calculated. Then we define and numerically calculate the escaping probability P_E , the probability that the treadmilling organism can escape from its image on the wall. This P_E does not take 0 or 1 value for any physically reasonable initial point. This suggests that the treadmilling organism feels the presence of its image on the wall even when it is placed at a position far from the wall at the initial time, and that, if the initial heading direction is appropriately chosen, it is possible for the microorganism to escape from the wall.

1 Introduction

The locomotion of microorganisms has received much attraction in fluid dynamics and Biology recently [1, 2]. As their motion possesses very small length scales and speeds, the dynamics is governed by low Reynolds number hydrodynamics,¹ where inertial forces are negligible in comparison to the viscous effects of the fluid.

Many studies have been undertaken on such dynamics in unbounded low Reynolds number flows [3, 4, 5]. In reality, however, most organisms are in the vicinity of other bodies or boundaries, where their hydrodynamic interactions with these have a significant effect on their motion. The importance of the existence of boundaries has also been suggested by many experimental observations. For example, some experimental observations [6, 7, 8] found a qualitative feature of microorganism near a solid wall to be attracted to no-slip boundaries. Berke *et al.* [9] measured the steady-state distribution of smooth-swimming *Escherichia Coli* (*E. Coli*) between two glass plates and found a strong increase of the cell concentration at the boundaries. They also theoretically demonstrated that hydrodynamic interactions of swimming cells with solid surfaces lead to their reorientation in the direction parallel to the surfaces, as well as their attraction to the closest wall. Lauga *et al.* [10] showed that circular trajectories are natural consequences of their force-free and torque-free swimming and hydrodynamic interactions with the boundary. This leads to a hydrodynamic

¹For example, the Reynolds number associated with the motion of *Escherichia coli* (*E. Coli*) is $O(10^{-4})$

trapping of the cells close to the surface. Drescher *et al.* [11] found that when two nearby Volvox colonies swim close to a solid surface, they attract one another and can form stable bound states in which they waltz or minuet around each other. These observations suggest that, in order to obtain a comprehensive understanding of low Reynolds number locomotions, it is necessary to study hydrodynamic interactions between microorganism and the boundaries.

Some of the phenomena stated above have already been verified by numerical simulations [12, 13]. However, not many physical explanations have been given to the locomotion of microorganism near boundaries. Berke *et al.* [9] studied the swimming microorganisms' attraction to boundaries by modeling the swimmer as a force dipole singularity. This simple model captures the attraction of the microorganisms to boundaries. However, contrary to the experimental findings, the microorganism in this model crashes into the boundary in finite time. Moreover, their analysis did not investigate the dynamics of microorganism near the boundary. Or and Murray [14] studied the dynamics of low Reynolds number swimming organism near a plane wall. They analysed the motion of a swimmer consisting of two rotating spheres connected by a thin rod, as a simple theoretical model of swimming organisms. They found that when the spheres are rotated in unequal velocities, the swimmer has a solution of steady translation parallel to the wall, and that under small perturbation, the swimmer exhibits wave-like motions along the wall. These results have recently been verified experimentally on a macroscale robotic prototype swimming in a highly viscous fluid [15]. Furthermore, Crowdy and Or [16] have proposed a singularity model for swimming microorganisms placed near an infinite no-slip boundary. Their model was based on a circular treadmilling organism which has no means of self-propulsion. They proposed the appropriate Stokes singularities that represented the flow field created by this treadmilling organism in the global fluid. By studying the interaction between these singularities and the no-slip wall, they formulated the nonlinear dynamics of the treadmilling organism explicitly, and fully characterised its motion near the wall. The trajectories parallel to the wall and periodic bouncing motion along the wall found in Crowdy and Or [16] had remarkable similarities to the trajectories shown in Or and Murray [14]. Crowdy and Samson [17], utilising the singularity model, investigated the dynamics of treadmilling organism near an infinite no-slip boundary with a gap of a fixed size. They employed a conformal mapping technique to avoid the difficulty in treating the image of the treadmilling organism on the wall. In their model, the treadmilling organism was found to make several qualitatively different trajectories; jumping over the gap, rebounding from the gap, trapping near the gap, and escaping the gap region even when the organism has the initial point in the gap. They also performed a bifurcation analysis as the size of the organism varies, and demonstrated a presence of stable equilibrium points in the gap region as well as Hopf bifurcations to periodic bound states. This reduced model system also exhibited a global gluing bifurcation in which two symmetric periodic orbits merge at a saddle point into symmetric bound states having more complex spatio-temporal structure.

The present project examines the dynamics of a treadmilling organism near a half-infinite no-slip wall (a corner whose angle is π). This is an important preliminary step to clarifying the dynamics of a treadmilling organism near a no-slip corner with an arbitrary angle, which will shed light on the cases with more complicated realistic geometries.

2 Two-dimensional Stokes flow problem and Goursat functions

2.1 General Solution for Stokes equation

In many of existing three-dimensional theoretical models of low Reynolds number locomotions, swimming microorganisms possess symmetry about their sagittal plane [14, 18] or even about their longitudinal axis [4, 5, 19]. This suggests that even in a fully three-dimensional flow, the motions of microorganisms are confined to a two-dimensional plane. Consequently, here we consider the two-dimensional model for a microorganism in a (x, y) -plane, in which we shall be free to treat the flow in a complex plane (z -space), where $z \equiv x + iy$. While the complex function method is one of the classical methods applied to ideal flows, a similar analytical method may also be applied to two-dimensional Stokes flows [20, 21]. Here, the complex method for Stokes flows is introduced to show that the two-dimensional Stokes flow is expressed through a couple of complex functions. This helps us to understand the flow clearly.

Stokes equations which describe the motion of an incompressible viscous fluid are

$$\begin{aligned}\nabla p &= \eta \Delta \mathbf{u}, \\ \nabla \cdot \mathbf{u} &= 0,\end{aligned}\tag{1}$$

where Δ is a Laplace operator, $\mathbf{u} = (u_x, u_y)$ is the fluid velocity, p and η are the pressure distribution and dynamic viscosity, respectively. As we are considering a two-dimensional flow, we can introduce the stream function ψ , such that the velocity is given by

$$u_x = \partial\psi/\partial y, \quad u_y = -\partial\psi/\partial x,\tag{2}$$

then the Stokes equations (1) reduce to biharmonic equation

$$\Delta^2\psi = 0.\tag{3}$$

Now we define complex velocity W as

$$\begin{aligned}u_x + iu_y &= \frac{\partial\psi}{\partial y} - i\frac{\partial\psi}{\partial x} \\ &= -2i\frac{\partial\psi}{\partial\bar{z}}.\end{aligned}$$

The vorticity $\omega = -\nabla^2\psi$ is then given by

$$\omega = -\nabla^2\psi = 2i\frac{\partial W}{\partial\bar{z}}.\tag{4}$$

By substituting (2) and (4) into the Stokes equations (1), we obtain

$$\frac{\partial p}{\partial x} = -\eta\frac{\partial\omega}{\partial y}, \quad \frac{\partial p}{\partial y} = \eta\frac{\partial\omega}{\partial x}.\tag{5}$$

The equations in (5) are the Cauchy-Riemann equations on the pair p and $-\eta\omega$. It follows that $p - i\eta\omega$ is an analytic function of z , and so that it can be written as

$$p - i\eta\omega = 4\eta f'(z),\tag{6}$$

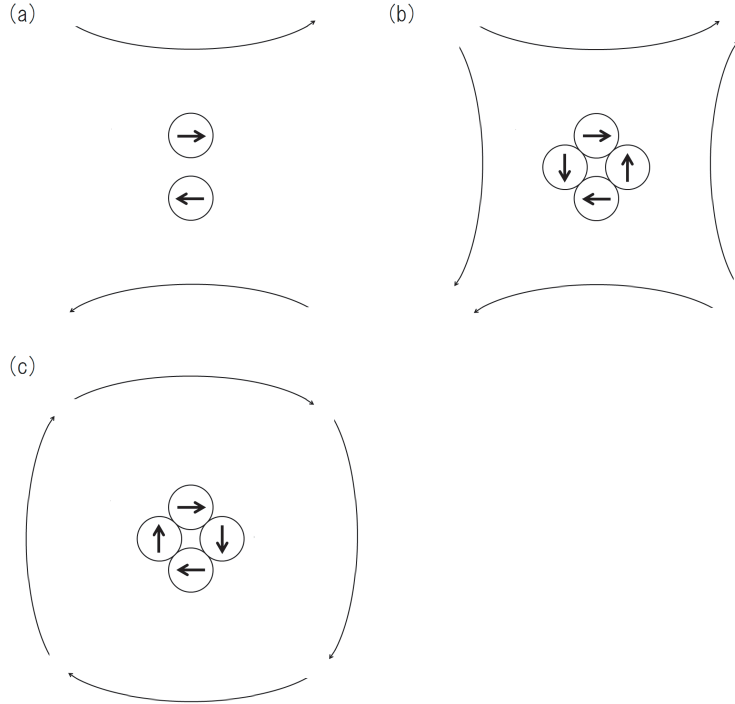


Figure 1: Schematic description of (a): Stokes dipole (b): stresslet (b): rotlet.

where $f'(z)$ is an arbitrary analytic function of z . Taking the imaginary part of (6), it is obvious that, by means of the function $f(z)$, ω can be written as

$$\omega = -4\text{Im} [f'(z)]. \quad (7)$$

Substituting (7) into (4) and integrating it with respect to z , we obtain

$$W = u_x + iu_y = f(z) + z\overline{f'(z)} + \overline{g'(z)}, \quad (8)$$

where $g'(z)$ is an arbitrary analytic function of z . Again, substituting (8) into (4) and integrating it with respect to z , we finally obtain the general solution for ψ in (3) as

$$\text{Im}[\bar{z}f(z) + g(z)]. \quad (9)$$

The functions $f(z)$ and $g(z)$, which are called Goursat functions, are analytic everywhere in the considered domain, except when isolated singularities are introduced in order to model various flows of interest. The functions $\bar{z}f(z)$ and $g(z)$ in (9) correspond to the viscous and potential part of the flow, respectively. Note that $g(z)$ does not appear (7), since potential flow has zero vorticity.

2.2 Singular solutions of Stokes flow

The Goursat functions $f(z)$ and $g(z)$ which determine the stream function of the flow are analytic almost everywhere in a considered domain except at isolated singular points. It is

necessary to choose appropriate singularities for the Goursat functions in order to describe the flow of interest. What kind of singularities should we use in order to model the flow generated by a treadmilling organism near a no-slip half-infinite wall? This is one of the main problems we should cope with for the formulation of the governing evolution functions of the treadmilling organism, and this will be discussed later in §3.1. Here in this section, the basic singularities of the Stokes flow are discussed. The flow generated by a treadmilling organism may be modeled with some of these singularities.

First of all, let us consider $f(z)$ of the form

$$f(z) = \mu \log(z - z_d), \quad (10)$$

where $\mu \in \mathbf{C}$ is the strength of the singularity. Then we insist that the complex velocity, given by (8),

$$\begin{aligned} u_x + iu_y &= -\mu \log(z - z_d) + \frac{\bar{\mu}z}{\bar{z} - \bar{z}_d} + \bar{g}'(\bar{z}) \\ &= -\mu \log(z - z_d) + \frac{\bar{z}(z - z_d)}{\bar{z} - \bar{z}_d} + \frac{\bar{\mu}z_d}{\bar{z} - \bar{z}_d} + \bar{g}'(\bar{z}) \end{aligned} \quad (11)$$

should be both single-valued and, at least, logarithmically singular at z_d . From these constraints, $g(z)$ should be chosen to have the form which satisfies

$$g'(z, t) = -\frac{\mu\bar{z}_d}{\bar{z} - \bar{z}_d} - \bar{\mu} \log(z - z_d). \quad (12)$$

Hence, if the Goursat functions $f(z)$ and $g(z)$ are

$$\begin{aligned} f(z) &= \mu \log(z - z_d) + \text{analytic function}, \\ g'(z) &= -\frac{\mu\bar{z}_d}{\bar{z} - \bar{z}_d} - \bar{\mu} \log(z - z_d) + \text{analytic function}, \end{aligned} \quad (13)$$

the flow described by these Goursat functions (13) is the one generated by Stokeslet at z_d . The complex velocity (11) takes the form

$$u_x + iu_y \sim -\mu \log |z - z_d|$$

and grows logarithmically as $z \rightarrow \infty$. This is the heart of the Stokes Paradox. In order to avoid the Stokes paradox, we must restrict our attention to Stokes flow problems which do not contain any Stokeslet. Note that imposing certain singularities to $f(z)$ forces g some concomitant singularities. Stokes dipole is obtained by superposing two Stokeslet, drawing infinitesimally close together, and with equal and opposite strengths tending to infinity at a rate inversely proportional to their separation. This is schematically shown in Fig.1 (a).

Next, if we allow $f(z)$ to have a simple pole at z_d ,

$$f(z) = \frac{\mu}{z - z_d}, \quad (14)$$

where $\mu \in \mathbf{C}$, and insist that the complex velocity, given by (8), should be singular like $1/|z - z_d|$, not like $1/|z - z_d|^2$. Then, again, the singularity in $f(z)$ forces $g(z)$ to have singularities, and we find that $g(z)$ should be chosen to have the form which satisfies

$$g'(z) = \frac{\mu\bar{z}_d}{(\bar{z} - \bar{z}_d)^2}. \quad (15)$$

This $g(z)$ corresponds to an irrotational dipole contribution of strength $-\mu\bar{z}_d$. If

$$\begin{aligned} f(z) &= \frac{\mu}{z - z_d} + \text{analytic function}, \\ g'(z) &= \frac{\mu\bar{z}_d}{(\bar{z} - \bar{z}_d)^2} + \text{analytic function}, \end{aligned} \tag{16}$$

we say that there is a stresslet of strength μ at z_d . This is given by the addition of two Stokes dipoles oriented at 90° with respect to each other as schematically shown in Fig.1 (b).

When $f(z)$ has singularities, as already stated above, $g(z)$ should have concomitant singularities to those in $f(z)$, but not conversely; $g(z)$ can have singularities which is independent of those of $f(z)$. These are kinematically identical to the singularities of the complex potential flow in two-dimensional incompressible and irrotational flow. Let us allow $g(z)$ to admit, for instance, a logarithmic singularity, which means simple pole in $g'(z)$,

$$g(z) = c \log(z - z_d), \tag{17}$$

where $c \in \mathbf{R}$ or $\in \mathbf{C}$. If $c \in \mathbf{R}$ z_d is a source/sink, whilst if $c \in \mathbf{C}$ z_d is a rotlet (or couplet). A rotlet is given by the difference between two Stokes dipoles oriented at 90° with respect to each other as schematically shown in Fig.1 (c), and this is kinematically identical to a point vortex [22]. Similarly, a double pole of $g'(z)$ corresponds to an irrotational dipole singularity, a triple pole corresponds to an irrotational quadrupole and so on.

With regard to modelling a swimming micro-organism, we are free to choose any combination of such Stokes flow singularities which seems to be appropriate for the problem at hand. However, each of these singularities will be a function of the swimmers size, shape, its swimming protocol and its local effect on the fluid around it. The attention is therefore focused on what specific combination of singularities can be used to accurately model a physical microorganism.

3 The model for a treadmilling tiny swimming organism

3.1 Basic settings and boundary conditions

Here we describe our simple model for a treadmilling organism. Any swimming organism in a Stokes flow locally generates a flow that can be modelled by some combination of Stokes flow singularities described in §2.2 placed on its position or its boundary. This singularity distribution is generally a complicated function of the swimming organism's basic properties such as size, shape, and configuration of cilia. The treadmilling organism does not have any self-propulsion in itself, but moves around in the considered domain when there is a boundary near it [6, 7, 10, 9, 11, 12, 13, 9, 14, 15, 16, 17]². It suggests that if a treadmilling organism is influenced by its surroundings such as other swimming organisms or a solid boundary, and behaves in a different way from when it is in isolation.

²Strictly, "treadmilling" and "swimming" describe different behaviours of the organism, and here in this project, we are only considering treadmilling organisms. However, as a treadmilling organism can move in the flow when there is a no-slip wall around it, we occasionally use the description "swimming organism" when we focus upon the organism's moving behaviour in the flow.

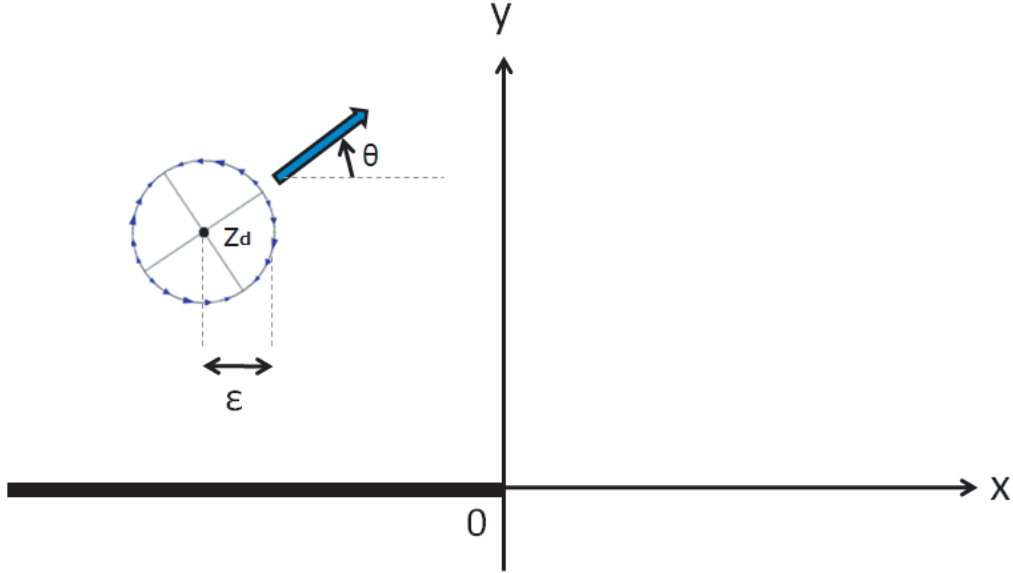


Figure 2: Simple model for a treading organism. z_d , ϵ , and θ are position of the organism, radius of the circular body of the organism, and the angle of the head of the organism from the real axis, respectively.

This means that, strictly speaking, the singularities in the Goursat functions referred above should be replaced by effective singularities, which will be complicated functions, according to the treading organism's surroundings. However, as a first approximation model of a treading organism's hydrodynamic interaction effects with a wall, it seems to be reasonable to consider the treading organism as passive. It follows that the treading organism always keeps its characteristics irrelevant to its surroundings.

In a simple theoretical model, we assume that the treading organism has a circle body of radius ϵ , with a moving centre $z_d(t) = x_d(t) + iy_d(t)$ in the fluid. We also assume that, with respect to the angle of the head of the treading organism from the real axis, $\theta(t)$, surface actuators of the treading organism induce a tangential velocity profile given by

$$\begin{aligned} U(\phi, t) &= 2V \sin(2(\phi - \theta)) \\ &= c(t) \exp(2i\phi) + \overline{c(t)} \exp(-2i\phi), \quad c(t) \equiv -iV \exp(-2i\theta(t)). \end{aligned} \quad (18)$$

Here V is a constant whose magnitude sets the time scale for the treading action, ϕ is the angle measured from the positive x direction and $\phi = \theta$ is the direction of the head of the treading organism (Fig.2). Note that when the treading organism produces a time-dependent tangential velocity profile, the Stokes equations imply that the fluid reacts to it instantaneously. Also note that in unbounded fluid, this velocity profile does not result in any self-propulsion of the organism due to its symmetry about real and imaginary axes.

The two Goursat functions $f(z, t)$ and $g(z, t)$, which give the stream function of the flow, should satisfy two boundary conditions: boundary conditions on the no-slip wall and

on the surface of the treadmilling organism. The boundary condition on the no-slip wall is, from (8),

$$u + iv = -f(z, t) + z\overline{f'(z, t)} + \overline{g'(z, t)} = 0 \quad \text{on the wall.} \quad (19)$$

Next, suppose that the centre of the treadmilling organism z_d moves in a translational velocity $\dot{x}_d(t) + i\dot{y}_d(t)$, and the organism rotates with an angular velocity $\omega(t)$. Then the boundary condition of the velocity field around the treadmilling organism can be written as

$$u_x + iu_y = -f(z, t) + z\overline{f'(z, t)} + \overline{g'(z, t)} = \dot{x}_d(t) + i\dot{y}_d(t) + [\epsilon\Omega + U(\phi, \theta(t))] \frac{dz}{ds}, \quad \text{at } \{z \mid |z - z_d| = \epsilon\}, \quad (20)$$

where dz/ds is the complex unit tangent to the boundary. Here, the relations

$$z - z_d = \frac{\epsilon^2}{\bar{z} - \bar{z}_d}, \quad \frac{dz}{ds} = i \frac{(z - z_d)}{\epsilon},$$

have been used.

3.2 Singularities of $f(z, t), g(z, t)$ and governing evolution equations of a treadmilling organism near a half-infinite wall

As it was mentioned in §2, the flow generated by a treadmilling organism in a Stokes flow can be locally modelled by some combination of Stokes flow singularities. However, it is not obvious what singularities should be chosen for each considered situation. A low Reynolds number treadmilling organisms exert no net force or torque upon the flow around it. Consequently, here we introduce a mathematical representation of the treadmilling organism as a two-dimensional stresslet, which is accompanied by additional singularities to those for the stresslet in its Goursat functions. Note that neither a Stokeslet nor a rotlet should be used for modelling the treadmilling organism, since the treadmilling organism should be force-free and torque-free. The type of the singularities in Goursat functions should be chosen such that the Goursat functions satisfy two boundary conditions (19) and (20). For this, we employ “image system method” [23, 16]. It is done by introducing additional singularities at $z = \bar{z}_d$, physically understood as the image of the treadmilling organism, to the Goursat functions.

The determination of the Goursat functions is basically performed by trial and error. Here we seek solutions for these Goursat functions having the form

$$\begin{aligned} f(z, t) &= \frac{\mu}{z - z_d(t)} + f_0 + f_1(z - z_d(t)) + \dots, \\ g'(z, t) &= \frac{b}{(z - z_d(t))^3} + \frac{a}{(z - z_d(t))^2} + \dots. \end{aligned} \quad (21)$$

$f(z, t)$ having no Stokeslet and $g(z, t)$ having no rotlet imply that the treadmilling organism is force-free and torque-free. Now we use the boundary condition (20) to find relations between the coefficients in (21) and the velocity of the treadmilling organism. On the surface of the treadmilling organism, where $|z - z_d| = \epsilon$,

$$z - z_d = \frac{\epsilon^2}{\bar{z} - \bar{z}_d}, \quad \frac{dz}{ds} = i \frac{z - z_d}{\epsilon}, \quad (22)$$

hold. Substituting (18) and (22) into (20) then equating coefficients of different powers of $z - z_d$, we obtain

$$\begin{aligned}
x_d + iy_d &= -f_0 + \overline{f_1}z_d + \overline{g_0}, \\
i\Omega &= -(f_1 - \overline{f_1}), \\
\mu &= -i\epsilon\overline{c}, \\
a &= \mu\overline{z_d}, \\
b &= \mu\epsilon - i\overline{c}\epsilon^3 = 2\mu\epsilon^2.
\end{aligned} \tag{23}$$

Thus the Goursat functions $f(z, t)$ and $g'(z, t)$ have the form

$$\begin{aligned}
f(z, t) &= \frac{\mu(t)}{z - z_d(t)} + f_0(t) + f_1(t)(z - z_d(t)) + \mathcal{O}((z - z_d(t))^2), \\
g'(z, t) &= \frac{2\mu(t)\epsilon^2}{(z - z_d(t))^3} + \frac{\mu(t)\overline{z_d(t)}}{(z - z_d(t))^2} + g_0(t) + \mathcal{O}((z - z_d(t))),
\end{aligned} \tag{24}$$

around z_d . This means that the treadmilling organism has an equivalent point singularity description with a stresslet of strength μ , corresponds to the terms $\mu/(z - z_d)$ in $f(z)$ and $(\mu z_d)/(z - z_d)^2$ in $g'(z)$, and the quadrupole of strength $2\epsilon^2\mu$ at z_d , corresponds to the term $(2\epsilon^2\mu)/(z - z_d)^3$ in $g'(z)$. Note that the existence of the quadrupole enables this model to describe a treadmilling organism with a finite size; for the pure point treadmilling organism, $\epsilon = 0$, the quadrupole vanishes. We also set the time scale of the motion by letting $V = \epsilon^{-1}$ so that

$$\mu(t) = \exp(2i\theta(t)). \tag{25}$$

Since the treadmilling organism is considered as a passive scalar here, the temporal change of its position follows the velocity of the fluid around it. Here, however, we should be aware that the velocity components which originates from the position of the treadmilling organism cannot affect the treadmilling organism itself by definition of ‘‘treadmilling’’. With these consideration, $\dot{z} = x_d + iy_d$ is given by the analytic part of the flow velocity (8) at $z = z_d$, and can be exactly written as

$$\frac{dz_d}{dt} = -f_0 + z_d\overline{f_1} + \overline{g_0}. \tag{26}$$

Similarly, the temporal change of the heading angle of the treadmilling organism is given from the half of the analytic part of the vorticity of the flow (7) at $z = z_d$:

$$\frac{d\theta}{dt} = -2\text{Im}[f_1]. \tag{27}$$

Hence, from (26) and (27), if we know f_0, f_1 , and g_0 of $f(z)$ and $g(z)$ that satisfy the conditions (19) and (20), we obtain the governing dynamical system of the treadmilling organism in an explicit form and know its trajectory.

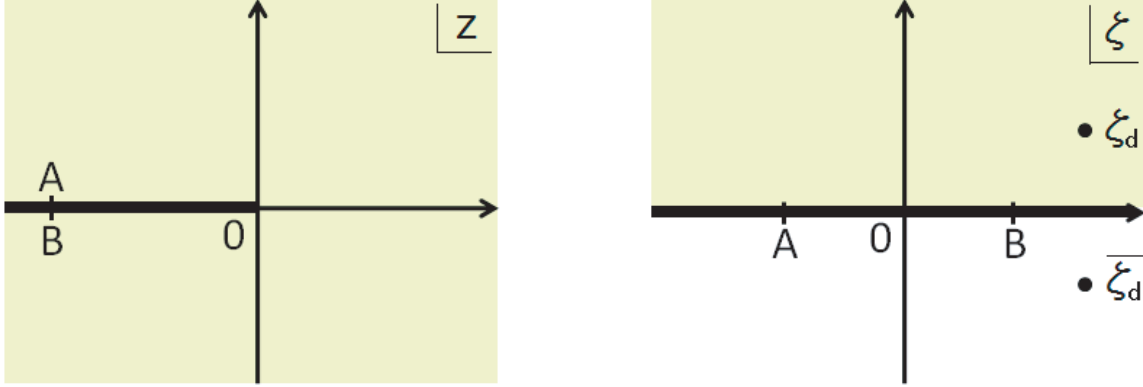


Figure 3: Considered domain in z -space and ζ -space. The points A and B in both spaces are mapped to each other by the conformal mapping $\zeta = iz^{1/2}$ and its inverse mapping $z = z(\zeta) = -\zeta^2$, then the infinite wall in ζ -space corresponds to the half-infinite wall in z -space.

3.3 Conformal mapping

The Goursat functions in (24) are the solution for the stream function for the flow generated in the vicinity of the treadmilling organism without accounting for the effect of the wall. To know the Goursat functions that have the form (24) near z_d and that also satisfy a boundary condition $u_x + iu_y = 0$ on the wall, we have to find the coefficients f_0, f_1 and g_0 such that the velocity satisfies the boundary condition on the wall. It, however, is not straightforward to determine such coefficients in a region near a half-infinite wall of an infinitesimal width in z -space, since where to place the image of the swimmer is not clear as we are now considering a half-infinite wall of infinitesimal width. To treat this complicated situation, here we employ conformal mapping techniques. Although the boundary value problem we have here is not conformally invariant, these techniques still work, since we always come and go to the two spaces.

let us consider a mapping

$$\zeta = iz^{1/2}. \quad (28)$$

This maps the domain $\{z \in \mathbf{C}\}$ to $\{\zeta \mid \text{Im}(\zeta) \geq 0\}$, especially, the domain $\{z \mid \text{Im}(z) = 0, \text{Re}(z) \leq 0\}$. The half-infinite wall we are considering in z -space are mapped to the domain $\{\zeta \mid \text{Im}(\zeta) = 0\}$, the infinite wall in ζ -space(Fig.3). The inverse of this conformal mapping (28) can be explicitly written as

$$z = z(\zeta) = -\zeta^2. \quad (29)$$

When written as a function of z , the function $\zeta(z)$ has the same type of point singularity with the one required for $f(z)$ and $g(z)$. It follows that ζ can serve as a uniformisation variable for the problem, and that if we define the composed functions

$$\begin{aligned} F(\zeta) &\equiv f(z(\zeta)), \\ G(\zeta) &\equiv g'(z(\zeta)), \end{aligned} \quad (30)$$

$F(\zeta)$ and $G(\zeta)$ can be written as single-valued functions of the variable ζ and are analytic except at the position of the isolated singularities we impose to these functions to describe

the treadmilling organism and its image. In other words, by utilising this uniformising ζ (ζ -space), we can write two analytic functions which determine the flow as single-valued functions with no branch point singularities.

From Crowdy and Or [16] and Crowdy and Samson [17], we propose the function $F(\zeta)$ to have the form

$$F(\zeta) = \frac{A}{\zeta - \zeta_d} + \frac{B}{(\zeta - \zeta_d)^3} + \frac{C}{(\zeta - \zeta_d)^2} + \frac{D}{(\zeta - \bar{\zeta}_d)} + E, \quad (31)$$

where we can set E to be zero without loss of generality because of an additive degree of freedom in the definition of $f(z)$. $\bar{\zeta}_d$ corresponds to the image of the swimmer on the wall, and in the ζ -space, this is simply a complex conjugate of ζ_d . Utilising this and the inverse mapping (29), we define the image of the swimmer in z -space as

$$\bar{z}_d \equiv \overline{z(\zeta_d)} \equiv z(\bar{\zeta}_d).$$

Recalling the non-slip boundary condition on the wall in z -space (19), $G(\zeta)$ should satisfy

$$\begin{aligned} G(\zeta) &= \overline{f(z)} - \bar{z}f'(z) \\ &= \overline{F(\zeta)} - \bar{z}\frac{d\zeta}{dz}F'(\zeta) \\ &= \overline{F(\zeta)} - (-i\zeta)^2\frac{1}{2}\zeta(-i\zeta)^{-2}F'(\zeta) \\ &= \overline{F(\zeta)} - \frac{1}{2}\zeta\overline{(-i\zeta)^2}(-i\zeta)^{-2}F'(\zeta), \end{aligned}$$

where, we have utilised the fact that $\bar{\zeta} = \zeta$ on the wall in ζ -space. Now, as $\zeta = |\zeta| \exp(i\phi)$, $\phi = 0$ or π on the wall,

$$\begin{aligned} \overline{(-i\zeta)^2}(-i\zeta)^{-2} &= \overline{[|\zeta| \exp(i(-\pi/2 + \phi))]^2 [|\zeta| \exp(i(-\pi/2 + \phi))]^{-2}} \\ &= [\exp(i(\pi - 2\phi))]^2 = 1 \end{aligned}$$

holds, so that

$$G(\zeta) = \overline{F(\zeta)} - \frac{1}{2}\zeta F'(\zeta). \quad (32)$$

By substituting (31) into (32), we obtain

$$\begin{aligned} G(\zeta) &= \frac{\bar{A}}{\zeta - \bar{\zeta}_d} + \frac{\bar{B}}{(\zeta - \zeta_d)^3} + \frac{\bar{C}}{(\zeta - \zeta_d)^2} + \frac{\bar{D}}{(\zeta - \zeta_d)} \\ &\quad - \frac{1}{2}\zeta \left[\frac{-A}{(\zeta - \zeta_d)^2} + \frac{-3B}{(\zeta - \zeta_d)^4} + \frac{-2C}{(\zeta - \zeta_d)^3} + \frac{-D}{(\zeta - \bar{\zeta}_d)^2} \right]. \end{aligned} \quad (33)$$

As $\bar{\zeta}_d$ is outside the considered domain in ζ -space, *i.e.* in the wall, $G(\zeta)$ only has singularity at $\zeta = \zeta_d$. Then it follows that $g(z)$ has singularities at $z = z_d$ and Moffatt type singularity[24] at $z = 0$.

Now we have to determine the unknown coefficients $A - D \in \mathbf{C}$. For A , we use the fact that $f(z(\zeta))$ has to have the singularity near z_d as shown in (24). Performing the Laurent expansion of $1/(\zeta - \zeta_d)$ in terms of z around z_d and comparing (24) and (31), we obtain

$$A = i \frac{\mu}{2z_d^{1/2}}. \quad (34)$$

To determine the rest of the unknown coefficients, $B - D$, we insist that g' has the required singularity structure in (24) at $z = z_d$. If we rewrite $G(\zeta)$ as a function of z and perform Laurent expansion in terms of z around z_d and compare it with $g'(z)$ in (24), we obtain

$$B = i \frac{\epsilon^2 \bar{\mu}}{4\bar{z}_d^{3/2}}, \quad (35)$$

$$C = \frac{\bar{\mu} (3\epsilon^2 - 4z_d\bar{z}_d + 4\bar{z}_d^2)}{8\bar{z}_d^2}, \quad (36)$$

$$D = i - \frac{\bar{\mu} (3\epsilon^2 - 4z_d\bar{z}_d - 4\bar{z}_d^2)}{8\bar{z}_d^{5/2}}, \quad (37)$$

and g_0 in (24),

$$\begin{aligned} g_0 = & -\frac{3\mu\bar{z}_d}{16z_d^2} + \frac{10\epsilon^2\mu}{32z_d^3} + \frac{3\epsilon^2\bar{\mu}}{8(z_d^{1/2} + \bar{z}_d^{1/2})^4 \bar{z}_d} \\ & - \frac{z_d - \bar{z}_d}{4(z_d^{1/2} + \bar{z}_d^{1/2})^3 z_d^{1/2}} - \frac{(-2z_d\bar{z}_d + 6\bar{z}_d^2 + 3\epsilon^2)\bar{\mu}}{16(z_d^{1/2} + \bar{z}_d^{1/2})^2 \bar{z}_d^2} \\ & - \frac{(-2z_d\bar{z}_d + 6\bar{z}_d^2 + 3\epsilon^2)\bar{\mu}}{16(z_d^{1/2} + \bar{z}_d^{1/2}) \bar{z}_d^{5/2}} \end{aligned} \quad (38)$$

Similarly, rewriting $F(\zeta)$ as a function of z and perform Laurent expansion in terms of z around z_d and compare with $f(z)$ in (24), and utilising (34) and (35)-(37), we obtain f_0 and f_1 ,

$$\begin{aligned} f_0 = & \frac{\mu}{4z_d} - \frac{\bar{\epsilon}^2\bar{\mu}}{4(z_d^{1/2} + \bar{z}_d^{1/2})^3 \bar{z}_d^{3/2}} + \frac{(2z_d\bar{z}_d - 2\bar{z}_d^2 - 3\bar{\epsilon}^2)\bar{\mu}}{8(z_d^{1/2} + \bar{z}_d^{1/2})^2 \bar{z}_d^2} \\ & - \frac{(-2z_d\bar{z}_d - 2\bar{z}_d^2 + 3\bar{\epsilon}^2)\bar{\mu}}{8(z_d^{1/2} + \bar{z}_d^{1/2}) \bar{z}_d^{5/2}}, \end{aligned} \quad (39)$$

$$\begin{aligned} f_1 = & \frac{1}{12z_d^2} \left(-\frac{3\mu}{4} + \frac{9z_d^{3/2}\bar{\epsilon}^2\bar{\mu}}{2(z_d^{1/2} + \bar{z}_d^{1/2})^4 \bar{z}_d^{3/2}} - \frac{3z_d^{3/2}(2z_d\bar{z}_d - 2\bar{z}_d^2 - 3\bar{\epsilon}^2)\bar{\mu}}{2(z_d^{1/2} + \bar{z}_d^{1/2})^3 \bar{z}_d^2} \right. \\ & \left. + \frac{3z_d^{3/2}(-2z_d\bar{z}_d - 2\bar{z}_d^2 + 3\bar{\epsilon}^2)\bar{\mu}}{4(z_d^{1/2} + \bar{z}_d^{1/2})^2 \bar{z}_d^{5/2}} \right). \end{aligned} \quad (40)$$

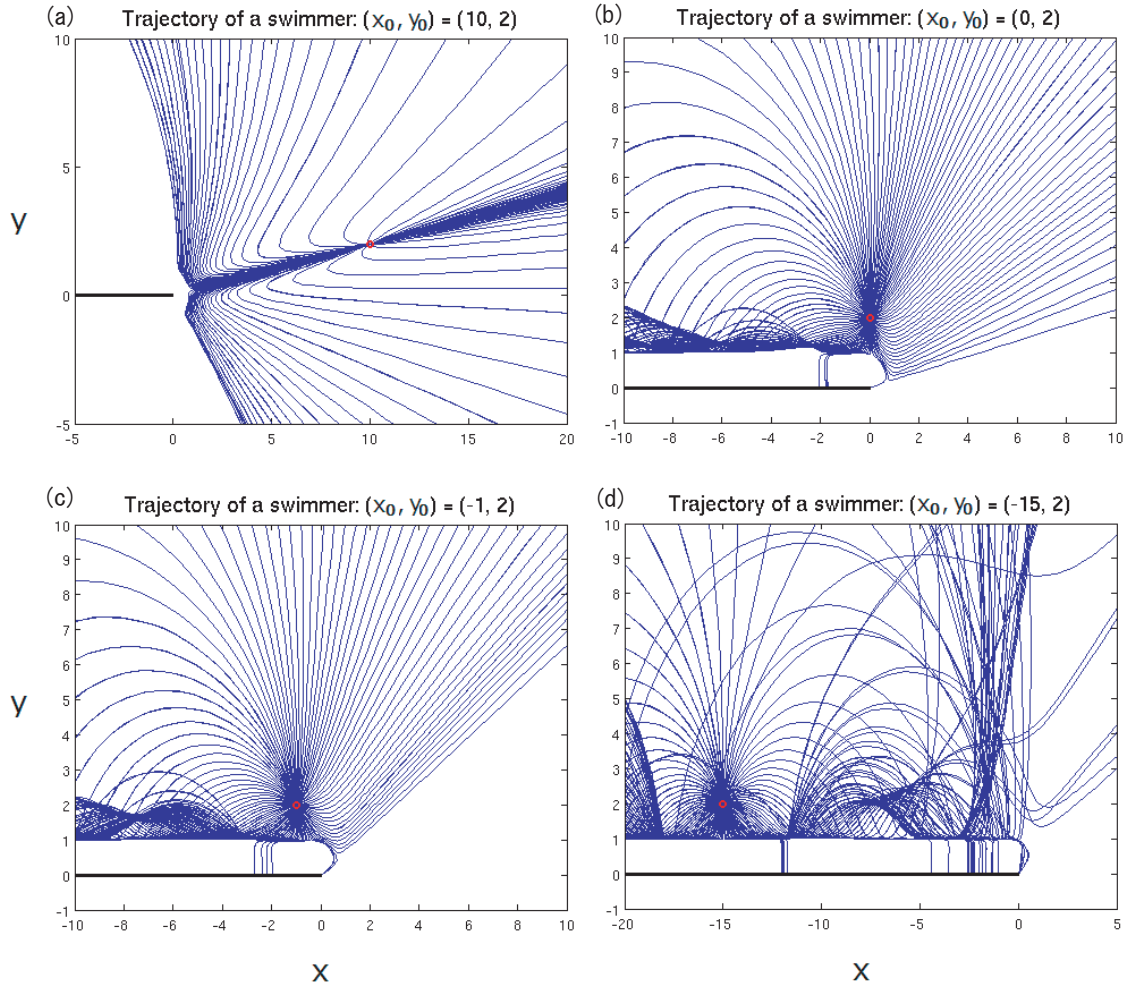


Figure 4: Examples of trajectories from the initial points (x_{d0}, y_{d0}) marked with red circles, each with 200 different initial heading directions θ_0 . (x_{d0}, y_{d0}) is (a):(10, 2), (b):(0, 2), (c):(-1, 2), and (d):(-15, 2).

4 Results of numerical simulations

Results of numerical simulations using the governing evolution equations for a treadmilling organism (26) and (27) are shown in this section. The time integration for all the simulations here were performed by Matlab ode45 solver with the absolute error tolerance 10^{-6} and relative error tolerance 10^{-3} . The radius of the circular body of the treadmilling organism ϵ is set to be unity, giving the reference length scale to the system. For initial conditions $(x_{d0}, y_{d0}, \theta_0)$, we took 3237 different $(x_{d0}, y_{d0}) \in [-20, 1] \times [1, 10] \oplus (1, 20] \times [0, 20]$ every 0.5 in both x and y direction, and 200 different $\theta_0 \in [0, 2\pi)$ every $\pi/100$.

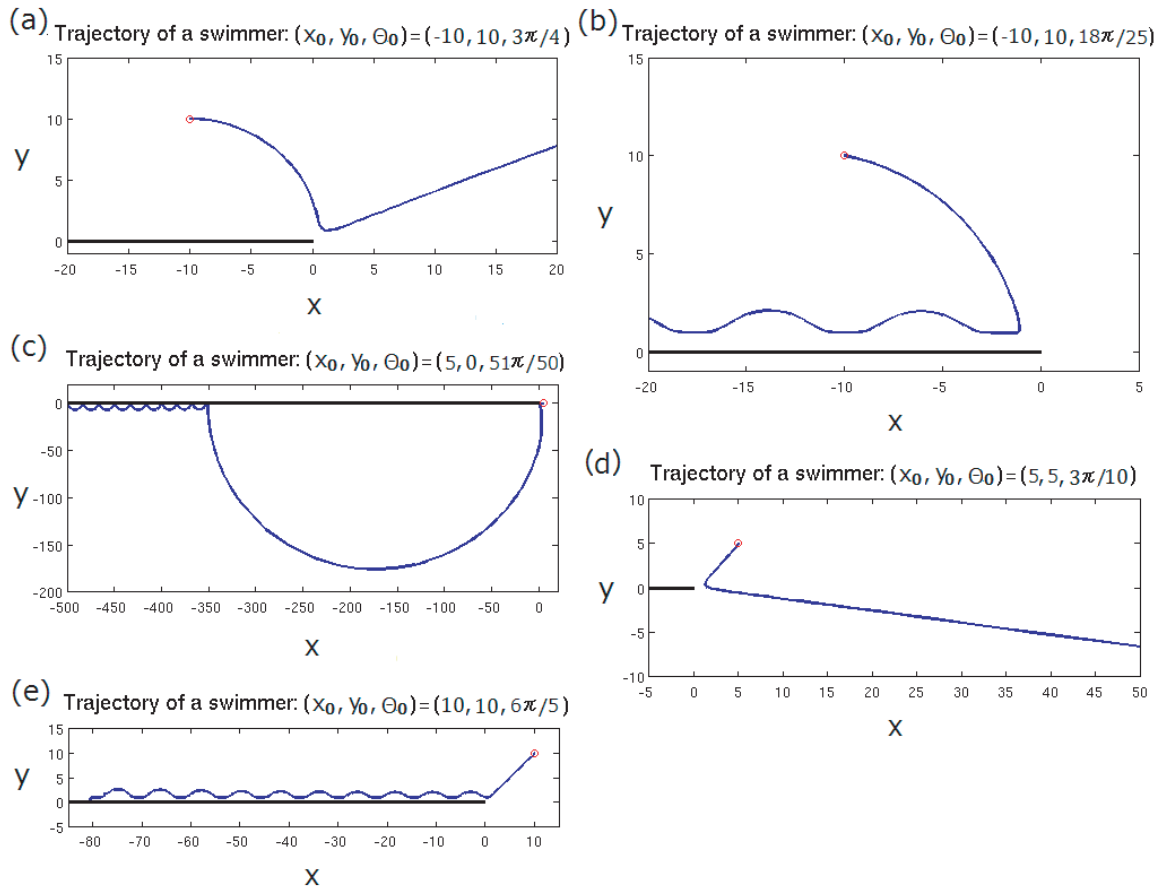


Figure 5: Examples of trajectories from the initial points (x_{d0}, y_{d0}) marked with red circles each, with a certain initial heading direction θ_0 . Treadmilling organism can escape from the wall, (a) and (d), be above the wall (b), be underneath the wall (d), or crush into the wall (e).

4.1 Various trajectories

By solving the governing equations of the swimming organism (26) and (27) utilising (38)-(40), we obtain many different trajectories depending upon different initial conditions. Figure 5 shows examples of such trajectories. At sufficiently large time, the treadmilling organism is possible to in any quadrant if we choose appropriate initial conditions, as we can see in Fig.5 (a)-(d). There also is a case that the treadmilling organism crushes into the wall in finite time as reported in [9]. An example of this unphysical trajectory is shown in Fig.5 (e), and will be discussed in §4.4. Both experimental observations and preceding theoretical studies suggest that, when there is a no-slip wall near a treadmilling organism, the organism tends to be attracted to its own image on the wall and move towards the wall [6, 7, 10, 9, 12, 13, 9, 16, 17]. This behaviour is clearly seen in all the trajectories shown in Fig.5 at an early stage of time integration. Nevertheless, in the cases shown in Fig.5 (a) and (d), the treadmilling organism moves away from the wall after it has come close to the edge of the wall once. Apparently, there are several cases that the treadmilling organism hangs around/above/underneath the wall as shown in Fig.5 (b) and (c). This is consistent with the results in several preceding study with a no-slip wall[6, 7, 10, 9, 12, 13, 9, 16, 17]. In these case, the treadmilling organism shows the trajectories bouncing along the wall as those in the case with an infinite no-slip wall[16], but the bouncing pattern is, unlike the case with the infinite no-slip wall, irregular and sometimes not periodic even after sufficiently large time has passed. This is also qualitatively consistent with the results of the study with a no-slip infinite wall with a gap [17]. Note that the treadmilling organism make changes its heading direction and the quality of its trajectory significantly when it arrived in the vicinity of the edge of the wall, where the image of the organism cannot move to the positive x-direction any more. Note also that, at a single glance, the initial heading direction θ_0 cannot be judged from the trajectory even approximately. This is a both natural and striking difference from the case with an infinite wall [16]. The strong asymmetry due to the absence of the wall in the region $x > 0$ gives a great influence to the trajectories, and even the trajectory for θ_0 doesn't make a straight vertical line. This feature can be clearly seen in Fig.4 in which 200 different trajectories for 200 different θ_0 for several combination of (x_{d0}, y_{d0}) are shown. In the cases with the initial point of the organism is close to or above the wall (Fig.4 (b)-(d)), it is somewhat possible to predict the direction that the treadmilling organism heads for at an early stage, but when the initial point is far from the wall (Fig.4 (a)), the heading direction is unpredictable from the knowledge of the trajectories for the cases with an infinite wall in [16]. However, we see a remarkable line on which many of the trajectories with different θ_0 seem to converge in all the cases in Fig.4, especially clearly in Fig.4 (a). This line may give us some kind of criterion in speculating the trajectory. As such lines seem to fall upon the lines which connect the edge of the wall $x = y = 0$ and the initial points of the treadmilling organism (x_{d0}, y_{d0}) which is marked by red circles in Fig.4, here, we introduce a critical linear line ℓ_c ,

$$\ell_c(x) \equiv \frac{y_{d0}}{x_{d0}}x. \quad (41)$$

Whether or not ℓ_c acts as a critical line in considering the direction of trajectory in the long run will be checked in §4.2. Another noticeable feature we can see from Fig.fig:AllThetas is the complexity of the trajectories for initial point with a large negative x-coordinate.

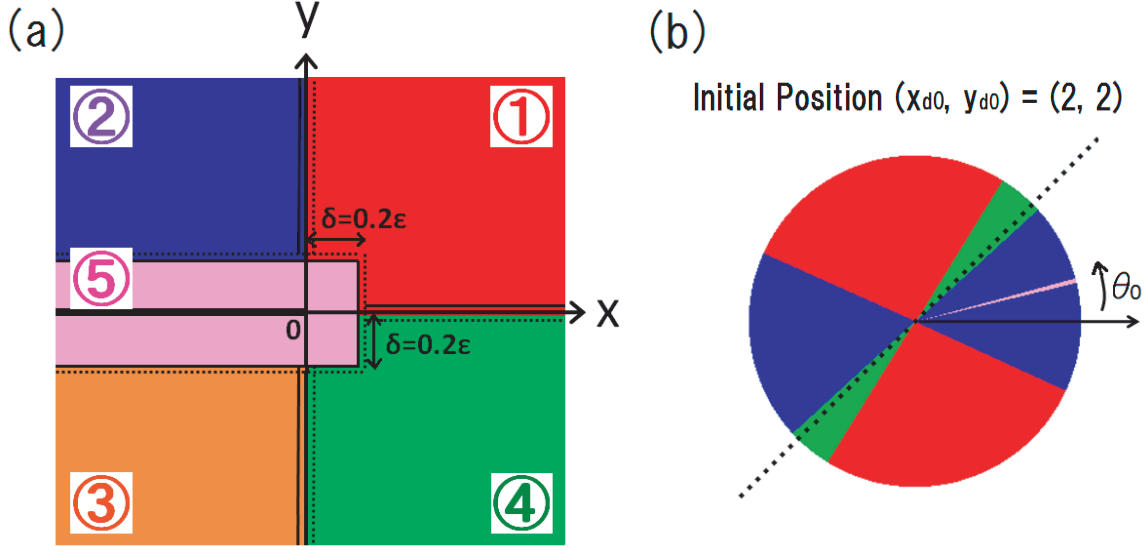


Figure 6: (a): Five regions. The thick black line corresponds to the wall. (b): An example of a pie chart. The different colours indicate in what region shown in the panel (a) the treadmilling organism from a certain initial point is at sufficiently large time. Dotted line corresponds to the slope of the critical line ℓ_c for the considered initial point.

As already seen in 5 and mentioned above, the treadmilling organism changes its heading direction and the quality of its trajectory greatly when it comes to the vicinity of the edge of the wall, $x = y = 0$. The behaviour of the organism after reaching such area significantly depends upon (x_d, y_d, θ) of the trajectory at the time. This makes the trajectories from large negative x_{d0} unpredictable and complicated. For such cases, even a very small difference in initial condition can result in a huge difference to the trajectory of the treadmilling organism, and this tendency is expected to become more distinct when the initial x-coordinate x_{d0} has larger negative value. We will come back this point in §4.2 again.

4.2 Escaping probability

Now, we classify a wide variety of trajectories in terms of the regions in which the treadmilling organism is at sufficiently large time. For this purpose, we first introduce five regions shown in Fig.6 (a). Region 1 is $\{(x, y) \in (0.2\epsilon, \infty) \times [0, 0.2\epsilon] \oplus (0, \infty) \times (0.2\epsilon, \infty)\}$, and is coloured red in Fig.6 (a). This is the region in which the treadmilling organism that escapes from the wall to $y \geq 0$ direction is. Region 2 is $\{(x, y) \in (-\infty, 0] \times (0.2\epsilon, \infty)\}$, and is coloured blue in Fig.6 (a). This is the region in which the treadmilling organism that goes back to above the wall is. Region 3 is $\{(x, y) \in (-\infty, 0] \times (-\infty, -0.2\epsilon)\}$, and is coloured orange in Fig.6 (a). This is the region in which the treadmilling organism that escapes from the wall to $y < 0$ direction is. Region 4 is $\{(x, y) \in (0.2\epsilon, \infty) \times [-0.2\epsilon, 0] \oplus (0, \infty) \times (-\infty, 0.2\epsilon)\}$, and is coloured green in Fig.6 (a). This is the region in which the treadmilling organism that goes back to underneath the wall is. Then Region 5 is $\{(x, y) \in (-\infty, 0.2\epsilon] \times [-0.2\epsilon, 0.2\epsilon]\}$, and is coloured pink in Fig.6 (a). This is to describe the case that the treadmilling organism

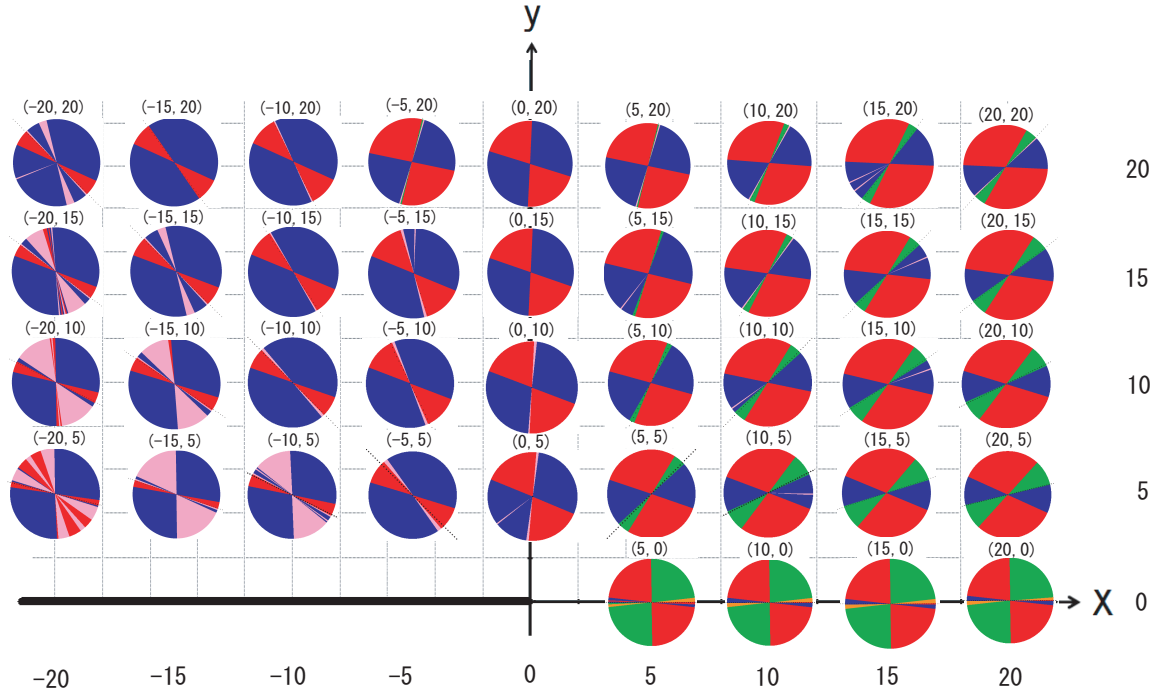


Figure 7: Pie charts at $t = 1500$ for several initial points. x and y coordinates of the point on which each pie chart is placed and correspond to the initial point for the pie chart. Thick black line represents the wall.

crushes into the wall.

Utilising these five regions, we make a pie chart for each considering initial point. The pie chart shows in what region the treading organism will be at a large time, here $t = 1500$, if it is given a certain initial heading direction θ_0 . An example of such pie chart is given in Fig.6 (b). Each colour appear in this pie chart corresponds to the colour given for each region in Fig.6 (a). The circular sector where the angle measured from the solid black arrow is in $[\theta_0 - \pi/200, \theta_0 + \pi/200]$ corresponds to the initial heading direction θ_0 of the treading organism, and the colour there indicate the region in which the treading organism is at sufficiently large time. For instance, the pie chart in Fig.6 (b) shows that the treading organism initially placed at the point $(x_{d0}, y_{d0}) = (2, 2)$ and given the heading direction $\theta_0 = 3/4\pi$ will be in the Region 1 at time $t = 1500$. The dotted black line in Fig.6 (b) corresponds to the slope of the critical line ℓ_c (41) for the considered initial point $(x_{d0}, y_{d0}) = (2, 2)$. This is to see whether or not, or to what degree, ℓ_c can act as a critical line in predicting the asymptotic position of the treading organism. For the initial position $(x_{d0}, y_{d0}) = (2, 2)$, we can see that, from Fig.6 (b), the dotted line fall near on the boundary between the blue(Region 2) and the green(Region 4) regions.

Figure 7 shows pie charts for several initial points (x_{d0}, y_{d0}) . The most impressive feature is the complex city of the pie charts for the initial points with large negative x-coordinates. This reflects the fact, which has been discussed in §4.1, that the treading organism changes its heading direction and the quality of its trajectory significantly when it has

come to the vicinity of the edge of the wall, $x = y = 0$ depending upon its (x_d, y_d, θ) at the time, and so even a very small difference in initial condition can result in a huge difference to its trajectory when the initial x-coordinate x_{d0} has large negative value. Note that, however, Pie charts tend to become rather simpler for larger y_{d0} for any fixed x_{d0} . One more thing we can easily notice is that there is some limitation for the region that the treadmilling organism is in at $t = 1500$ depending upon its initial position. Broadly, the treadmilling organism is in regions 1, 2, or 5 when its $(x_{d0}, y_{d0}) \in [-20, 0] \times [1, 10]$; regions 1, 2, 4, or 5 when its $(x_{d0}, y_{d0}) \in (0, 20] \times [1, 10]$; regions 1, 2, and 4 when $x_{d0} \in (0, 20], y_{d0} = 0$. The possibility of going the region 3 where is underneath the wall that the cases the initial y position y_{d0} is zero is natural because of the symmetry about $y = 0$ they have. When we compare the pie charts at a certain x-coordinate, it is apparent that the pie charts become simpler for larger y_{d0} . This is because of the effect of asymmetry that the wall gives to the system. Also, although all the pie charts almost have 2-fold rotational symmetry, desymmetrised part becomes obvious when the initial point is near the wall, where the asymmetric effect of the system becomes strong. From the pie charts in Fig.7, it is apparent that ℓ_c does not act as a critical line as we expected in §4.1 in any way in considering the position of the treadmilling organism at sufficiently large time, at least at $t = 1500$. However, ℓ_c still falls near one of the boundaries of two different regions in the cases with positive initial x-coordinate $x_{d0} > 0$ and in the cases whose initial positions are far from the wall.

Now let us consider the escaping probability P_E , the probability that the treadmilling organism can escape from the wall, or its own image on the wall. Although, ideally, this is to be defined by means of the positions of the treadmilling organism at $t \rightarrow \infty$, here we define this P_E as the probability of the treadmilling organism's being in the region 1 or 4 at sufficiently large time $t = t_l$, *i.e.*,

$$P_E \equiv \frac{\{\#\theta_0 \mid z_d \in \text{regions 1 or 4 at } t = t_l\}}{\#\theta_0}. \quad (42)$$

The escaping probability P_E for $t_l = 1500$ for different initial conditions are shown in Fig.8, where each (x, y) coordinate corresponds to each considered initial position of the treadmilling organism. P_E takes the value $0 < P_E < 1$ for almost all the initial positions in Fig8; P_E is zero for only several points with $(x_{d0} < 0, y_{d0} = 0)$, which is the case that the treadmilling organism touches the wall at the initial time and rather meaningless in this context, and there is no point where P_E is unity. This suggests that treadmilling organism has the possibility of both escaping from the wall and being above/underneath the wall for any initial position. Even when the treadmilling organism is initially placed at a position far from the wall, it feels the presence of its own image on the wall and move towards the wall if its initial heading direction θ_0 is properly chosen. Similarly, even when the treadmilling organism is initially placed at a point with large negative x-coordinate, above the wall and far from the edge of the wall, for some θ_0 , it finally moves away from its own image on the wall. The distribution and the monotonic change of the value of P_E in the region where $x > 0$ seems to be reasonable. However, in the region where $x < 0$, there are couple of lines which has larger P_E value than naive expectation. This might be the result of the complex pie charts in these region, but the reason why we see such fairly larger P_E value on the points on certain lines is not clear and needs further investigations.

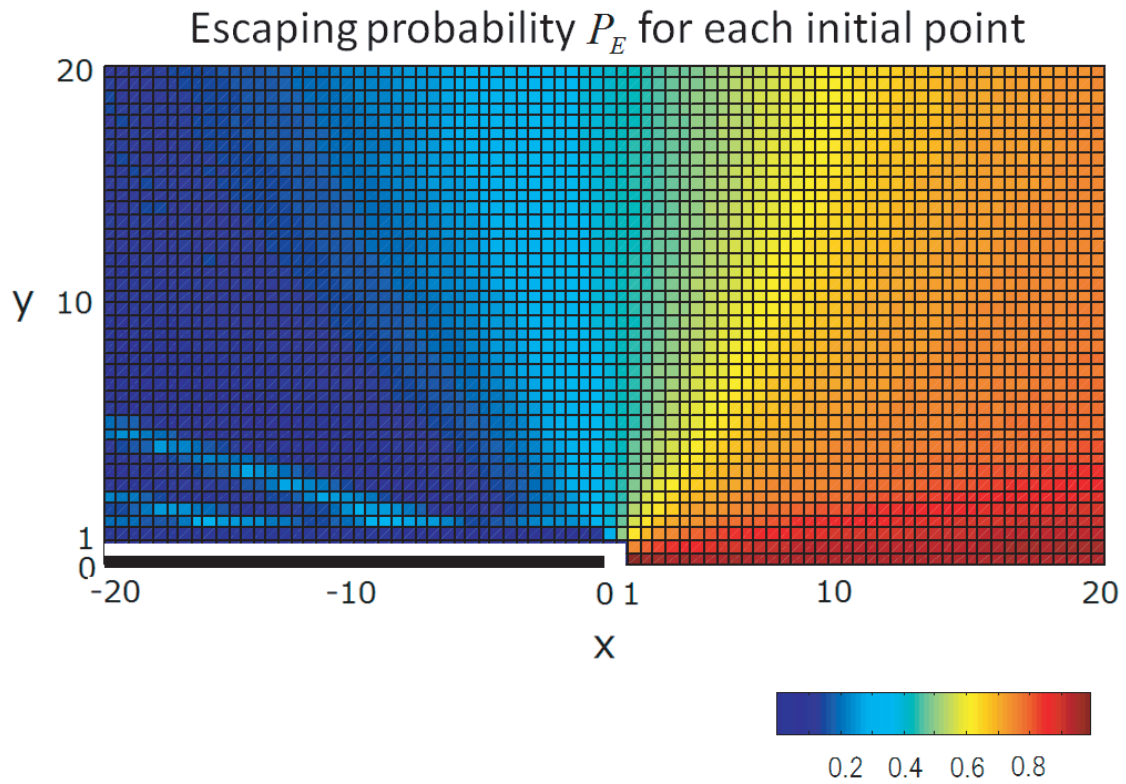


Figure 8: Escaping probability at $t = 1500$ for different initial points. Each (x, y) coordinate and the thick black line corresponds to the considered initial position of the treadmilling organism and the wall, respectively.

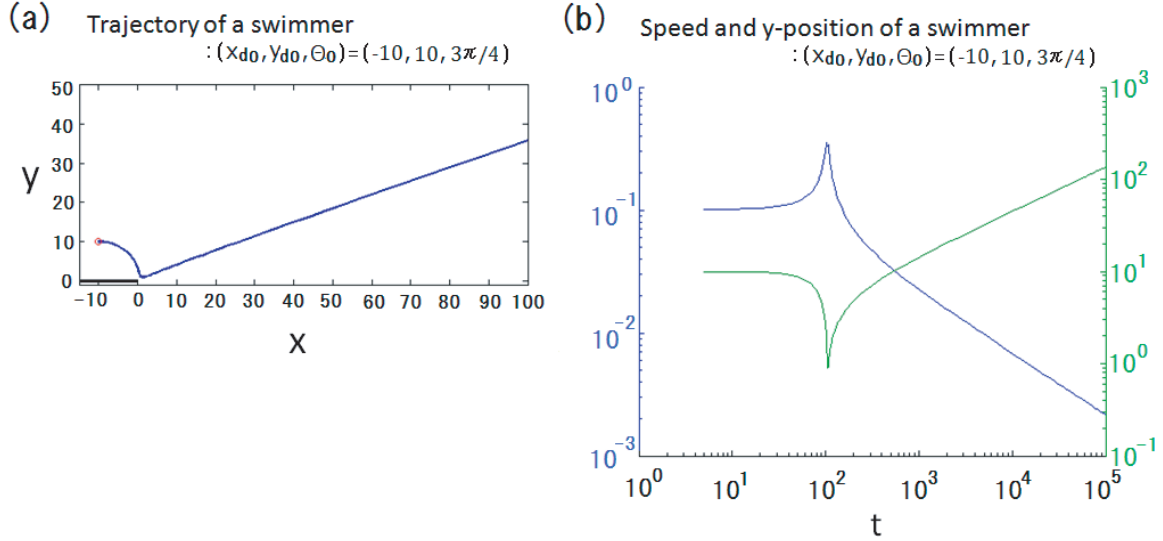


Figure 9: Trajectory of the temporal change of the speed of the treadmilling organism for the case initial condition $(x_{d0}, y_{d0}, \theta_0) = (-10, 10, 3\pi/4)$. (a): the trajectory (b): the temporal variation of the y-coordinate of the organism z_d (blue solid line) and the temporal variation of the speed of the organism (green solid line).

4.3 Temporal change of the speed of the treadmilling organism in region 1 and 4

For the definition of the escaping probability P_E in §4.2, we have considered the probability of the treadmilling organism's being in the region 1 or 4 at large time $t = t_l$. Then the following questions may always exit: has the treadmilling organism surely escaped from the wall when it is in these region at large time?, does it stop if it reaches a point sufficiently far from the wall? An example of the temporal variation of the speed of the treadmilling organism $\sqrt{\dot{x}_d^2 + \dot{y}_d^2}$ is shown in Fig.9. When the treadmilling organism comes in the vicinity of the edge of the wall and changes its heading direction, the speed of the organism shows a steep increase. After that the treadmilling organism moves away from the wall. Then, as the distance from the wall increase, the moving speed of the organism decreases. The speed is $\sim 10^{-2}$ at $t \sim 10^3$ and keep decreasing. This is because that the farther away from the wall the treadmilling organism goes, the effect of its image on the wall becomes weaker since the image cannot follow the organism any further than the edge of the wall. Nevertheless, we cannot be perfectly sure whether or not the speed of the treadmilling organism approaches zero as $t \rightarrow \infty$, and whether or not the treadmilling organism has really escaped from the wall in this case, only from Fig.9. To confirm these points, we need a longer time integration with much higher accuracy; this should be a further work.

4.4 Velocity field

Fig.10 shows the velocity field calculated from the two Goursat functions when the treadmilling organism is placed at the point $(x, y) = (2, 2)$. It can be confirmed from Fig.10(a)

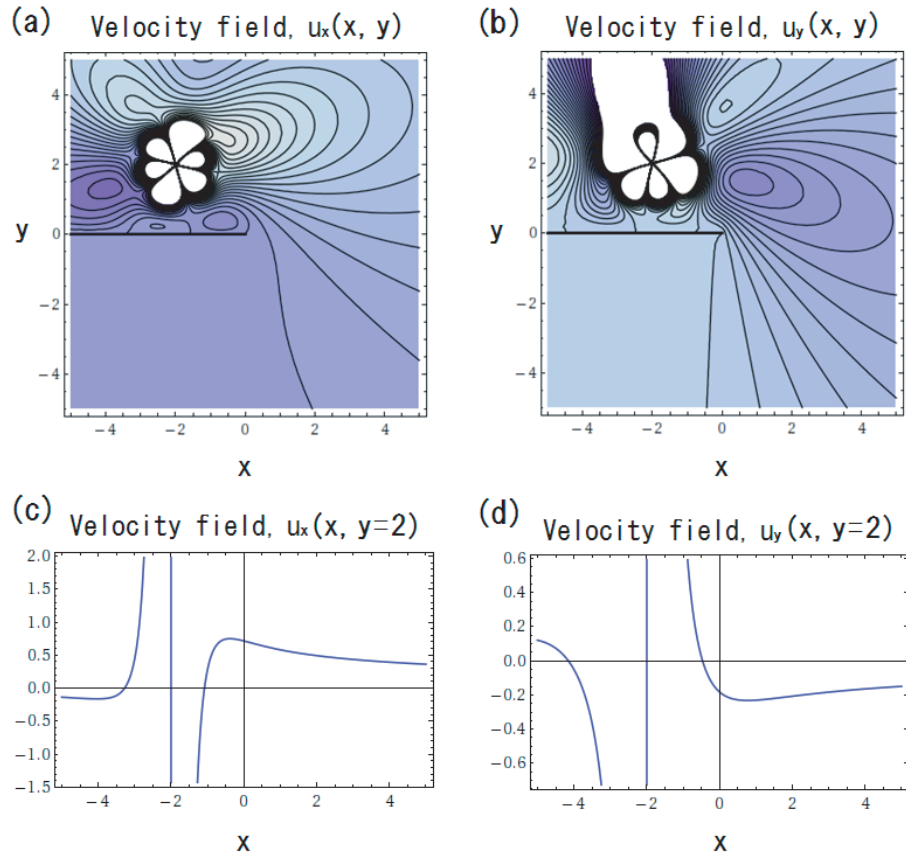


Figure 10: Velocity field when the treadmilling organism is at the point $(x, y) = (2, 2)$. (a) and (b): x-velocity $u_x(x, y)$ (b) : y-velocity $u_y(x, y)$ (c): x-velocity at $y = 2$ $u_x(x, y = 2)$ (d): y-velocity at $x = 2$ $u_y(x = 2, y)$. The darkness of colour represents the value of the velocity, the thin and the thick solid line are contour of the velocity and the no-slip wall, respectively.

and (b) that the boundary condition on the no-slip wall is satisfied, and the velocity diverges at the point $(x, y) = (2, 2)$ where the singularity, which represents the treadmilling organism, is placed. The boundary condition on the surface of the treadmilling organism, on the contrary, is not satisfied; the contours of the both x- and y- velocity are not circles around the treadmilling organism. This is because the model used in this project is very simple and has failed to capture all the features of the treadmilling organism we need to consider. This may affect the behaviour of the treadmilling organism, especially when it is near the wall. This may be one of the reasons why we had unphysical trajectories such as the treadmilling organism crushes into the wall. Nevertheless, at least for the case that the treadmilling organism bounces back on the wall, we have confirmed that the qualitative behaviour of the organism does not change even when the model which shows better boundary condition. This suggests that it may probably be possible to consider that the trajectories, apart from those that the treadmilling organism crushes into the wall, we have found in this report are reasonable.

5 Discussion and conclusions

The governing evolution equations for a treadmilling organism when there is a half-infinite non-slip wall in the considered unbounded domain have been derived, by means of an image system method, in §3. The treadmilling organism was assumed to have a circle body of radius ϵ and a moving centre $z_d(t) = x_d(t) + iy_d(t)$ in such a domain. It has been modelled as an equivalent point singularity description with stresslet of strength μ and the quadrupole of strength $2\epsilon^2\mu$ at z_d in Stokes flow. The existence of the wall of an infinitesimal thickness causes a critical problem when an image system method is employed; it is not straightforward to determine where to place the image of the treadmilling organism on the wall. To avoid this problem, a conformal mapping $\zeta - iz^{1/2}$ was employed, which maps $\{z \in \mathbf{C}\}$ to $\{\zeta \mid \text{Im}(\zeta) \geq 0\}$, especially, the half-infinite wall in z -space to the infinite wall in ζ -space. Then z_d and its image were defined through ζ_d , the image of ζ_d on the infinite wall in ζ -space *overline* ζ_d , and the conformal mapping. By imposing two boundary conditions, one on the body of the organism and the other on the no-slip wall, the coefficients of two Goursat functions $f(z, t)$ and $g(z, t)$, which gives the stream function of the flow, were determined. The governing evolution equations of the position and the heading direction of the treadmilling organism, z_d and θ_d , were obtained by taking the analytic part of the flow velocity and the half of the analytic part of the vorticity of the flow, respectively.

The trajectories of the treadmilling organism were numerically calculated in §4. The different trajectories of the treadmilling organism depending upon different initial conditions were discussed in §4.1. The treadmilling organism was attracted to its image on the wall, as suggested in previous experimental and theoretical studies [6, 7, 10, 9, 12, 13, 9, 16, 17], at an early stage of the time integration. Nevertheless, in some cases, the treadmilling organism moved away from the wall after it had come to the vicinity of the edge of the wall once. To investigate this behaviour further, in the first part of §4.2, we have divided \mathbf{R}^2 domain into five regions and made pie charts which show in what region the treadmilling organism is at sufficiently large time. The pie charts for different initial positions provided in §4.2, demonstrated that those for the initial points with larger negative x-coordinates have more complex structures compared to those with smaller negative x-coordinates. This

reflects the fact that the treadmilling organism changes in its heading direction and the quality of its trajectory significantly when it comes to the vicinity of the edge of the wall, $x = y = 0$ depending upon its (x_d, y_d, θ) at the time, and that even a very small difference in initial condition can make a huge difference to its trajectory when the initial x-coordinate x_{d0} has larger negative value as seen in §4.1. We further defined and numerically calculated the escaping probability P_E , the probability that the treadmilling organism can escape from the wall, or its image on the wall in the latter part of §4.1. This P_E did not take 0 or 1 value for any physically reasonable initial point. This suggests that treadmilling organism has the possibility of both escaping from the wall and being above/underneath the wall for any initial position. Even when the treadmilling organism is initially placed at a position far from the wall, it feels the presence of its image on the wall and move towards the wall if its own initial heading direction θ_0 is appropriately chosen. Similarly, even when the treadmilling organism is initially placed at a point with large negative x-coordinate, above the wall and far from the edge of the wall, for some θ_0 , it can finally move away from its own image on the wall. When the treadmilling organism moves away from the wall, its speed decreases as the distance from the wall increases as discussed in §4.3. This is because that the treadmilling organism feels less effect of its own image on the wall as it moves farther from the wall, since the image cannot follow the organism any further than the edge of the wall.

The results in this project seem reasonable in some respects. However, the obtained P_E does not take 0 or 1 for any physically reasonable initial point, even with large positive/negative x-coordinate. This may suggest that the combination of the singularities used required some modifications when the treadmilling organism was far from the edge of the wall. The situation with a half-infinite no-slip wall in an unbounded domain corresponds to the case in which the no-slip wall has a gap as studied in [17] but of an infinite width. Checking whether or not the results gained in this report and those for the case with no-slip wall with a gap in the limit of width of the gap $\rightarrow \infty$ may help us gain some further understanding of this problem. The behaviour of a treadmilling organism near a 90° no-slip corner or even a no-slip corner with arbitrary angle in an unbounded domain will be our next problem to investigate. These will be an important step to clarifying how a treadmilling organism behaves and the effect of its mixing when it is in a bounded domain with no-slip boundaries of complicated forms.

Acknowledgements

I would like to thank the Woods Hole Oceanographic Institution for the opportunity to participate in Geophysical Fluid Dynamics Program 2010. I would also like to express my sincere gratitude to Jean-Luc Thiffeault for his great patience, and for the fruitful discussions. My thanks also goes to Matthew Finn for his helpful advice and suggestions. Last but not least, I would like to say a big thank you to the staff members and the fellows, without whom the programme would have been much less fruitful.

Some of the numerical calculations for this project were performed on the computer systems of the Institute for Information Management and Communication (IIMC) of Kyoto University.

References

- [1] Lauga, E. and T.R. Powers, "The hydrodynamics of swimming micro-organisms", *Rep. Prog. Phys.*, **72**, 096601 (2009)
- [2] Pedley, T. J. and J. O. Kessler, "Hydrodynamic phenomena in suspensions of swimming microorganisms", *Annu. Rev. Fluid Mech.*, **24** 313 (1992)
- [3] Shapere, A. and F. Wilczek, "Geometry of self-propulsion at low Reynolds numbers", *J. Fluid Mech.*, **189**, 557 (1989)
- [4] Najafi, A. and R. Golestanian, "Simple swimmer at low Reynolds number: Three linked spheres", *Phys. Rev. E*, **69** 062901 (2004)
- [5] Avron, J. E., O. Kenneth, and D. H. Oakmin, "Pushmepullyou: an efficient microswimmer", *New J. Phys.*, **7**, 234 (2005)
- [6] Rothchild, A. J., "Non-random distribution of bull spermatozoa in a drop of sperm suspension", *Nature(London)*, **198**, 1221 (1963)
- [7] Winet, H., G.S. Bernstein, and J. Head, "Observations on the response of human spermatozoa to gravity, boundaries and fluid shear", *Reprod. Fert.*, **70**, 511523 (1984)
- [8] Cosson, J., P. Huitorel, and C. Gagnon, "How spermatozoa come to be confined to surfaces", *Cell Motil. Cytoskel.*, **54**, 5663 (2003)
- [9] Berke, A. P., L. Turner, H. C. Berg, and E. Lauga "Hydrodynamic attraction of swimming microorganisms by surfaces", *Phys. Rev. E*, **101**, 038102 (2008)
- [10] Lauga, E., W. R. DiLuzio, G. M. Whitesides, and H. A. Stone, "Swimming in circles: motion of bacteria near solid boundaries", *Biophys. J.*, **90**, 400 (2006)
- [11] Drescher, K., K. C. Leptos, I. Tuval, T. Ishikawa, T. J. Pedley, and R. E. Goldstein, "Dancing Volvox: Hydrodynamic Bound States of Swimming Algae", *Phys. Rev. Lett.*, **102**, 168101 (2009)
- [12] Ramia, M., D.L. Tullock, and N. Phan-Thien, "The role of hydrodynamics interaction in the locomotion of microorganism", *Biophys. J.*, **65**, 755 (1993)
- [13] Hernandez-Ortiz, J. P., C.G. Stoltz, and M.D. Graham, "Transport and collective dynamics in suspensions of confined swimming particles", *Phys. Rev. Lett.*, **95**, 204501 (2005)
- [14] Or, Y. and R. M. Murray, "Dynamics and stability of a class of low Reynolds number swimmers near a wall", *Phys. Rev. E*, **79** 045302 (2009)
- [15] Zhang, S., Y. Or, and R.M. Murray, "Experimental demonstration of the dynamics and stability of a low Reynolds number swimmer near a plane wall", *Proc. Amer. Cont. Conf.* (accepted)

- [16] Crowdy, Darren. and Yazhar Or, "Two-dimensional point model of a low-Reynolds-number swimmer near a wall", *Phys. Rev. E*, **81** 030313 (2010)
- [17] Crowdy, Darren. and Ophir Samson, "Hydrodynamic bound states of a low-Reynolds-number swimmer near a gap in a wall", *J. Fluid.Mech.* (accepted)
- [18] Becker, L. E., S. A. Koehler, and H. A. Stone, "Hydrodynamic attraction of swimming microorganisms by surfaces", *J. Fluid Mech.*, **490**, 15 (2003)
- [19] Leshansky, A. M. and O. Kenneth, "Surface tank treading: Propulsion of Purcell's toroidal swimmer", *Phys. Fluids*, **20** 063104 (2008)
- [20] Imai, I., "*Ryuutai Rikigaku (Fluid Dynamics)*", Shokabo, Tokyo (1973)
- [21] Milne-Thomson, L. M., "*Theoretical Hydrodynamics, Fifth Edition*", The Macmillan And Company, New York, pp.683-684, (1996)
- [22] Batchelor, G. K., "*An introduction to fluid dynamics*", Cambridge University Press, Cambridge (1967)
- [23] Blake, J. R. and A. T. Chwang, "Fundamental singularities of viscous flow. part 1: the image systems in the vicinity of a stationary no-slip boundary", *J. Eng. Math.*, **8**, 23 (1974)
- [24] Moffatt, H. K., "Viscous and resistive eddies near a sharp corner", *J. Fluid Mech.*, **18**, 1 (1964)